Temperature independent resistance response for mixed conducting SrFeyCozOx thin films

Tunney, Jim; Post, Michael; Du, Xiaomei; Yang, Dongfang

Publisher's version / Version de l'éditeur:

Electrochemical Society Proceedings, 2000-32, pp. 476-487, 2000

MARIA CLANCY
DGO
INST FOR CHEM PROCESS & ENVIR TECH
NATIONAL RESEARCH COUNCIL CANADA
M-12, ROOM 141, 1200 MONTREAL RD.
OTTAWA, ON K1A 0R6
CANADA

Client Number:	MARIA E. CLANCY
Title:	**SOLID STATE IONIC DEVICES II - CERAMIC SENSORS**
Author:	WACHSMAN, E.D.; WEPPNER, W.; TRAVERSA, E.; VANYSEK, P. ET AL. EDITORS
Date:	2000
Pages:	476-487
Article Title:	TEMPERATURE INDEPENDENT RESISTANCE RESPONSE FOR MIXED CONDUCTING SRFEYCOZOX THIN FILMS (2000)
Article Author:	TUNNEY, J.J.; POST, M.L.
Publisher:	ELECTROCHEMICAL SOCIETY PROCEEDINGS VOLUME 2000-32

INSTRUCTIONS: NEEDED BY: 24 JUNE 2009

Estimated cost for this 12 page document: $0 document supply fee + $0 copyright = $0

Phone/Téléphone: 1-800-668-1222 (Canada - U.S./E.-U.) (613) 998-8544 (International)
www.nrc.ca/cisti Fax/Télécopieur: (613) 993-7619 www.cnrc.ca/icist
info.cisti@nrc.ca info.icist@nrc.ca

National Research Council Canada / Conseil national de recherches Canada

TEMPERATURE INDEPENDENT RESISTANCE RESPONSE FOR MIXED CONDUCTING $SrFe_yCo_zO_x$ THIN FILMS

James J. Tunney, Michael L. Post, Xiaomei Du and Dongfang Yang
Institute for Chemical Process and Environmental Technology
National Research Council of Canada
Montreal Road, Ottawa, Ontario, K1A 0R6, Canada

A series of $SrFe_yCo_zO_x$ thin films on sapphire substrates were prepared by laser deposition, and the conductance responses to both temperature and gas composition in O_2/N_2 mixtures were examined. All films exhibited *p*-type semiconductor behaviour with film conductivities at 500 °C between 20-200 S/cm for films exposed to 100% O_2 atmosphere and 0.4-25 S/cm for films exposed to 0.2 % O_2. At 500 °C, thin films of compositions $SrFe_yCo_{1-y}O_x$, $0.25 \leq y \leq 0.75$, were found to be the most conductive for oxygen partial pressures between $0.002 < p(O_2) < 1.0$ atmospheres. $SrFeO_x$ and $SrFe_{1.3}Co_{0.2}O_x$ films were found to be the least conductive under these conditions. $SrFe_{0.25}Co_{0.75}O_x$ and $SrFe_{0.5}Co_{0.5}O_x$ films were found to exhibit regions of temperature independence between $200 \leq T \leq 500$ °C for oxygen partial pressures between 0.2 % to 100 % O_2. This temperature independence was interpreted as the result of a balancing of two opposing thermal effects: thermal activation of charge carriers and thermal induced oxygen stoichiometry changes within the film. For some films, enhanced oxygen sensitivity was observed over narrow $p(O_2)$ regions, and is attributed to cubic perovskite to brownmillerite phase transitions.

INTRODUCTION

Mixed conducting ceramic materials of the type $SrFe_yCo_zO_x$ are characterized by their oxygen non-stoichiometry and their high electronic and ionic conductivities (1-15). Consequently, they are suitable candidate materials for applications such as oxygen separation membranes, electrode materials for solid oxide fuel cells and solid state chemical sensors. It has been reported that some $SrFe_yCo_{1-y}O_x$ materials have oxygen ion mobilities greater than yttria stabilized zirconia (YSZ) below 800 °C (1-3,7). Recently, the high oxygen ion mobility of the $SrFe_yCo_{1.5-y}O_x$ ($1.0 < y < 1.5$) composition (8-17) has been attributed to the perovskite type $SrFe_yCo_{1-y}O_x$ phase (8).

It has previously been shown that perovskite-based ceramic materials which exhibit *p*-type semiconductivity and mixed conductivity may be suitable candidates for temperature independent gas sensors (18-21). The basis for this temperature independence is the balancing of two separate thermal effects. The first effect is related to the thermal activation of charge carriers and is described in Eq. [1] (18):

$$\sigma = \sigma_o \exp(-E_A / kT) \qquad [1]$$

An Arrhenius relationship exists between the conductivity of the material (σ) and the temperature (T) and is characterized by an activation energy E_A. For a *p*-type

ANCE RESPONSE FOR MIXED
O_x THIN FILMS

nei Du and Dongfang Yang
vironmental Technology
il of Canada
K1A 0R6, Canada

re substrates were prepared by
onses to both temperature and
amined. All films exhibited *p*-
nductivities at 500 °C between
$_2$ atmosphere and 0.4-25 S/cm
C, thin films of compositions
to be the most conductive for
$< p(O_2) < 1.0$ atmospheres.
nd to be the least conductive
nd $SrFe_{0.5}Co_{0.5}O_x$ films were
ependence between $200 \leq T \leq$
en 0.2 % to 100 % O_2. This
as the result of a balancing of
vation of charge carriers and
ges within the film. For some
observed over narrow $p(O_2)$
cite to brownmillerite phase

TION

ype $SrFe_yCo_zO_x$ are characterized by
ronic and ionic conductivities (1-15).
als for applications such as oxygen
lid oxide fuel cells and solid state
$Fe_yCo_{1-y}O_x$ materials have oxygen ion
SZ) below 800 °C (1-3,7). Recently,
$1.0 < y < 1.5$) composition (8-17) has
hase (8).
ased ceramic materials which exhibit
may be suitable candidates for
The basis for this temperature
al effects. The first effect is related to
ibed in Eq. [1] (18):

[1]

luctivity of the material (σ) and the
tivation energy E_A. For a *p*-type

iety Proceedings Volume 2000-32

semiconductor, an increase in temperature normally results in increased conductivity caused by an increase in the number of hole electronic carriers in the conduction band. This results from the thermal excitation of electrons from the conduction band to a higher energy band. The second thermal effect is related to the oxygen non-stoichiometric properties of some perovskite materials. A temperature increase for a constant O_2 partial pressure in the gas phase over the solid results in some degree of oxygen evolution and an associated reduction of the material:

$$O^x \rightarrow V_o^{\bullet\bullet} + 2e^- + 1/2O_2\uparrow \qquad [2]$$

Equation [2] describes the removal of an oxygen atom from an oxygen site, O^x, yielding two electrons, a doubly charged oxygen vacancy, $V_o^{\bullet\bullet}$, and O_2 gas. The electrons which are produced by the evolution of oxygen combine with the dominant electronic hole carriers, decreasing the conductivity of the material.

Under certain circumstances it has been shown that it is possible to balance these two opposing thermal effects, so that the resistance response of the semiconductor material is effectively temperature independent This has been examined with the goal of developing temperature independent gas sensors (18-21). Williams *et. al.* examined a series of ferrates including $BaFe_{1-x}Ta_xO_3$, which showed negligible conductivity dependence to temperature, between 600-800°C (18-20). More recently, Moos *et. al.* demonstrated that acceptor and donor doped $SrTi_{1-x}Fe_xO_{3-\delta}$ materials could be tailored to yield temperature independent conductivity responses between 700-900 °C (21). These materials were being investigated for applications as oxygen sensors for combustion exhaust control.

Thick film perovskite materials were used for all of these studies, and the temperature independent regions were above 500 °C. Thin films provide advantages related to the higher surface area to volume ratio. Thinner films of gas sensors based on a bulk equilibration mechanism between the film and the gas mixture provide faster response times. Previous work has shown that it is possible to grow high quality thin films of $SrFeO_x$ ($2.5 \leq x \leq 3.0$) using pulsed laser deposition (PLD) which show gas sensing properties between 350-500 °C (22-25).

For some gas sensing applications, it would be advantageous to use transducer materials which exhibit a temperature independent resistance response at lower temperatures, and that still show adequate gas sensitivity. In this study, $SrFe_yCo_zO_x$ materials grown as thin films are shown to have rapid and reversible bulk oxygen equilibration properties which may be exploited to achieve a conductivity response for gas sensing which has a negligible temperature dependence.

EXPERIMENTAL

All $SrFe_yCo_zO_x$ materials were prepared as sintered pellets using standard ceramic techniques (22-25). High purity (>99.99%) $SrCO_3$, Fe_2O_3, and Co_3O_4 materials were mixed in the required ratios, followed by thermal treatments in flowing argon and/or oxygen at 1050-1100 °C. These materials were then pressed into 12 mm diameter targets followed by sintering at 1000-1150°C under flowing oxygen. The pellets were all verified to be single phase by X-ray diffraction before being used as targets for pulsed laser ablation deposition (PLD). The X-ray spectra were indexed according to previously

determined crystal structures. $SrFe_yCo_{1-y}O_x$ (y= 0.25, 0.5, 0.75, 0.9, 1.0) were indexed to the cubic perovskite structure (26-28), $SrCoO_x$ to the hexagonal structure (29), and $SrFe_{1.0}Co_{0.5}O_x$ and $SrFe_{1.3}Co_{0.2}O_x$ were both indexed to an orthorhombic phase which is an intergrowth of repeating layers of perovskite and rock-salt layers (9,12,30).

Two series of $SrFe_yCo_zO_x$ thin films on $(1\bar{1}02)$ single crystal sapphire substrates were prepared by laser deposition using a Lambda-Physik LPX305*i* laser operating at λ = 248 nm. These included the solid solution perovskite series $SrFe_yCo_{1-y}O_x$ (y=0, 0.25, 0.5, 0.75, 0.9, 1.0) and the structurally related materials $SrFe_{1.0}Co_{0.5}O_x$ and $SrFe_{1.3}Co_{0.2}O_x$. For each composition, the films were deposited at two separate thicknesses, approximately 30 nm and 300 nm. A laser pulse rate of 8 Hz was used with an energy density at the target of 1.5 $J{\cdot}cm^{-2}$. During the deposition step, the sapphire substrate was heated at 700 °C under a background gas of 13 Pa oxygen, followed by cooling at approximately 10°C/min in a background oxygen pressure of 53 kPa.

X-ray spectra for both pellets and films were collected using a Scintag D2000 diffractometer over the range $20 \leq 2\Theta \leq 80°$ using graphite monochromated Cu-Kα radiation. Film thicknesses were estimated based on stylus profiler measurements taken with a Dektak IIA instrument on masked 300 nm $SrFe_yCo_zO_x$ thin films grown on sapphire. Elemental analysis for targets and films were performed by inductively coupled plasma atomic emission spectroscopy (ICP-AES) using standard solutions to determine the ratio of Sr, Fe and Co elements. Scanning electron microscopy (SEM) images were taken of the as-deposited films using a JEOL JSM 5300 instrument.

Electrical conductivity measurements of the films were taken using a 2-wire method in a controlled environment where the temperature could be varied between 20-600 °C and the composition of the flowing gas changed as required. High purity ($[O_2] + [N_2] >$ 99.99%) gas mixtures flowing at 220 cm^3/min in a 1 litre volume chamber were used for all tests. Electrical contacts were achieved by thermally depositing 200 nm Au pads directly onto the $SrFe_yCo_{1-y}O_x$ films. Experimental details are provided elsewhere (23,25).

In order to determine the dynamic temperature dependences, the resistances of the films were measured while cooling at a controlled rate of 10 °C/min from 500-100 °C. Previous to this, the films were equilibrated at 500 °C for at least three hours in one of two flowing O_2/N_2 gas mixtures: 0.2 % O_2 or 100 % O_2. The composition of the flowing gas mixture was invariant throughout the cooling cycle. For each film, this procedure was repeated at least twice to ensure reproducibility. The conductivities of the films as a function of the O_2/N_2 gas mixtures were measured isothermally at 500 °C. This was done by measuring the film resistances as the O_2/N_2 gas mixtures were varied from oxygen poor (~ 0.01 % O_2) to oxygen rich (100 % O_2) conditions in a stepwise manner, typically waiting 60 minutes before changing to the next O_2/N_2 gas composition. The gas mixtures were then changed in the reverse order from oxygen rich to oxygen poor in order to verify reversibility.

0.25, 0.5, 0.75, 0.9, 1.0) were indexed to
O_x to the hexagonal structure (29), and
dexed to an orthorhombic phase which is
and rock-salt layers (9,12,30).
($1\bar{1}02$) single crystal sapphire substrates
da-Physik LPX305*i* laser operating at λ =
'skite series $SrFe_yCo_{1-y}O_x$ (y=0, 0.25, 0.5,
erials $SrFe_{1.0}Co_{0.5}O_x$ and $SrFe_{1.3}Co_{0.2}O_x$.
posited at two separate thicknesses,
se rate of 8 Hz was used with an energy
position step, the sapphire substrate was
13 Pa oxygen, followed by cooling at
n pressure of 53 kPa.
were collected using a Scintag D2000
using graphite monochromated Cu-Kα
d on stylus profiler measurements taken
) nm $SrFe_yCo_zO_x$ thin films grown on
s were performed by inductively coupled
S) using standard solutions to determine
lectron microscopy (SEM) images were
M 5300 instrument.
films were taken using a 2-wire method
ure could be varied between 20-600 °C
as required. High purity ($[O_2] + [N_2] >$
a 1 litre volume chamber were used for
thermally depositing 200 nm Au pads
mental details are provided elsewhere

ture dependences, the resistances of the
ed rate of 10 °C/min from 500-100 °C.
00 °C for at least three hours in one of
0 % O_2. The composition of the flowing
cycle. For each film, this procedure was
. The conductivities of the films as a
d isothermally at 500 °C. This was done
gas mixtures were varied from oxygen
nditions in a stepwise manner, typically
O_2/N_2 gas composition. The gas mixtures
xygen rich to oxygen poor in order to

RESULTS AND DISCUSSION

Film Composition and Structure

XRD analysis of the 300 nm films deposited on sapphire showed the films to be crystalline and textured (Figure 1). No reflections for the 30 nm films were observed except for the very strong sapphire reflections from the substrate due to the small sample size of these films. The $SrFe_yCo_{1-y}O_x$ (y= 0.5, 0.75, 0.9, 1.0) films were all indexed to the cubic perovskite structure (26) and were (110) textured. The $SrFe_{0.75}Co_{0.25}O_x$ film showed an additional degree of (111) texturing. The $SrCoO_x$ film (Figure 1f) was indexed to the $SrCoO_x$ hexagonal structure and was textured (201) (29). It was not clear from the $SrFe_{0.25}Co_{0.75}O_x$ film (Figure 1e) if it adopted the cubic perovskite or the hexagonal

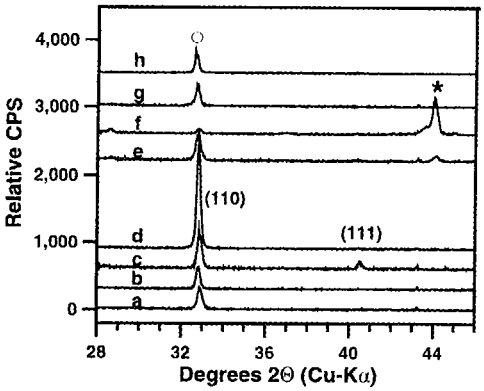

Figure 1: X-ray spectra for 300 nm thin films of $SrFe_{0.5}Co_{0.5}O_x$ on sapphire: a) $SrFeO_x$; b) $SrFe_{0.9}Co_{0.1}O_x$; c) $SrFe_{0.75}Co_{0.25}O_x$; d) $SrFe_{0.5}Co_{0.5}O_x$; e) $SrFe_{0.25}Co_{0.75}O_x$; f) $SrCoO_x$; g) $SrFe_{1.0}Co_{0.5}O_x$; h) $SrFe_{1.3}Co_{0.2}O_x$. Indexing is given for the cubic perovskite structure.; indicates (201) $SrCoO_x$ hexagonal phase indexing.

structure. Likewise, the $SrFe_{1.0}Co_{0.5}O_x$ and $SrFe_{1.3}Co_{0.2}O_x$ films could not be unambiguously assigned to the expected orthorhombic phase, since the reflection at $2\Theta \approx 32.7°$ could be indexed to either the (110) reflection of the cubic perovskite structure or to the composite (400)+(002) or (251) reflections of the orthorhombic phase (9,12,30).

SEM analysis of all the 30 nm films showed the films to be featureless and smooth at a length scale $\geq 0.1\mu m$. The 300 nm films showed some texture with SEM with grain boundaries and/or scaling being observed at a length scale (l), of $1 \leq l \leq 5$ μm for $SrFe_yCo_{1-y}O_x$ (y = 0.25, 0.5, 0.75, 0.9, 1.0) compositions. The $SrCoO_x$, $SrFe_{1.0}Co_{0.5}O_x$ and $SrFe_{1.3}Co_{0.2}O_x$ films showed no evidence of scaling but showed some roughness at a length scale of $0.1 \leq l \leq 0.3$ μm. Elemental analysis of the films showed that the Sr, Fe, and Co metallic elements occurred in the correct ratios to within the 5% estimated error limits of the ICP-AES technique. XRD, elemental and SEM analyses confirmed that PLD is a suitable technique for the stoichiometric transfer of material from the target to the substrate for complex metal oxides such as mixed conducting $SrFe_yCo_zO_x$ ceramics.

Dependence of Temperature on Film Conductivity

The conductance response to temperature for two 30 nm thick films ($SrFeO_x$ and $SrFe_{0.25}Co_{0.75}$) is shown in Figure 2 as a set of Arrhenius plots. The higher conductivity of both films in 100% O_2 compared to 0.2% O_2 confirm that these materials are *p*-type semiconducting oxides (18). It is also evident that the conductance response to

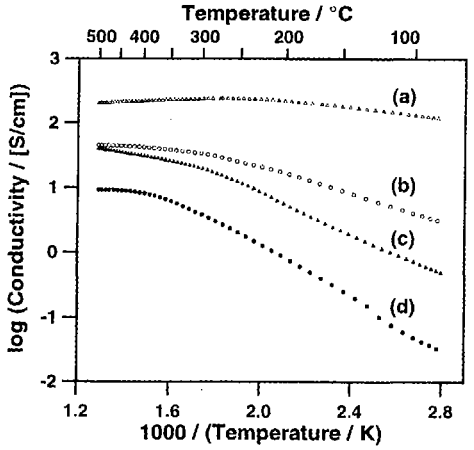

Figure 2: Arrhenius plots for two 30 nm thick films in two O_2/N_2 mixtures. $SrFe_{0.25}Co_{0.75}O_x$ in: a) 100 %, c) 0.2% O_2; and $SrFeO_x$ in: b) 100 %; d) 0.2% O_2.

temperature is much smaller for $SrFe_{0.25}Co_{0.75}$ than for $SrFeO_x$ especially in the temperature range $200 \leq T \leq 500$ °C. An activation energy parameter, E_A, related to this temperature dependence of film conductance has been extracted from the Arrhenius plots

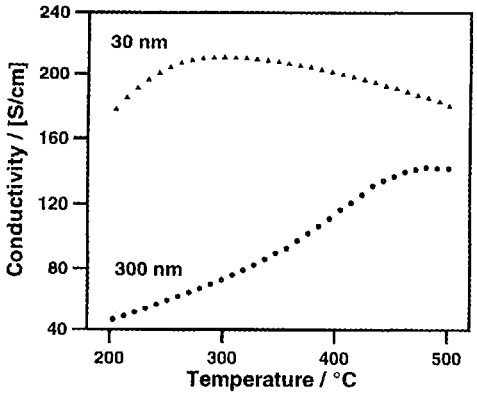

Figure 3: Effects of films thickness on the conductance response with temperature for two $SrFe_{0.5}Co_{0.5}O_x$ films. Cooling ramps were carried out in 100% O_2 at 10 °C/min.

of the entire $SrFe_yCo_{1-y}O_x$ series of films. The results summarized in Table 1, show the E_A values which were calculated for two temperature ranges. The $350 \leq T \leq 500$ °C "non-stoichiometric" range was chosen since at these temperatures, bulk oxygen equilibration of the film is possible. Consequently, the balancing of the thermal activation of charge

ity

for two 30 nm thick films ($SrFeO_x$ and rrhenius plots. The higher conductivity of confirm that these materials are *p*-type ent that the conductance response to

Figure 2: Arrhenius plots for two 30 nm thick films in two O_2/N_2 mixtures. $SrFe_{0.25}Co_{0.75}O_x$ in: a) 100 %, c) 0.2% O_2; and $SrFeO_x$ in: b) 100 %; d) 0.2% O_2.

.75 than for $SrFeO_x$ especially in the tion energy parameter, E_A, related to this been extracted from the Arrhenius plots

Figure 3: Effects of films thickness on the conductance response with temperature for two $SrFe_{0.5}Co_{0.5}O_x$ films. Cooling ramps were carried out in 100% O_2 at 10 °C/min.

esults summarized in Table 1, show the ture ranges. The $350 \leq T \leq 500$ °C "non- temperatures, bulk oxygen equilibration cing of the thermal activation of charge

carriers effect with the "non-stoichiometric" effect can occur (Equation 1-2). By comparison, the $100 \leq T \leq 200$ °C "stoichiometric" range was chosen since the oxygen stoichiometry for the films is expected to be quenched when the experimental cooling rate of 10 °C/min was used.

Table I: Activation energies of conduction, E_A, for $SrFe_yCo_zO_x$ films on sapphire in the "non-stoichiometric" (350-500 °C) and "stoichiometric" (200-100°C) temperature ranges. E_A values were derived from dynamic 10 °C/min temperature cooling ramps.

Composition	**Thickness** (nm)	**E_A / eV (350-500 °C)** 100% O_2	0.2% O_2	**E_A / eV (100-200 °C)** 100% O_2	0.2% O_2
$SrFeO_x$	300	0.39	0.39	0.23	0.47
	30	0.04	0.09	0.22	0.44
$SrFe_{0.9}Co_{0.1}O_x$	300	0.37	0.19	0.28	0.49
	30	0.10	0.12	0.22	0.39
$SrFe_{0.75}Co_{0.25}O_x$	300	0.20	-0.04	0.18	0.31
	30	-0.02	0.01	0.13	0.29
$SrFe_{0.5}Co_{0.5}O_x$	300	0.13	0.10	0.12	0.26
	30	-0.04	-0.003	0.12	0.26
$SrFe_{0.25}Co_{0.75}O_x$	300	0.002	0.04	0.16	0.25
	30	-0.04	0.12	0.08	0.31
$SrCoO_x$	300	0.06	0.02	0.15	0.18
	30	0.07	-0.005	0.17	0.17
$SrFe_{1.3}Co_{0.2}O_x$	300	0.08	0.21	0.22	0.34
	30	0.23	0.31	0.25	0.39
$SrFe_{1.0}Co_{0.5}O_x$	300	0.02	0.10	0.19	0.32
	30	0.07	0.064	0.19	0.29

In general, higher level of cobalt substitution results in smaller temperature dependences, with the smallest E_A values reported for the $SrFe_{0.75}Co_{0.25}O_x$, $SrFe_{0.5}Co_{0.5}O_x$ and $SrFe_{0.25}Co_{0.75}O_x$ films. It is also noteworthy that the temperature dependences of the films exposed to 0.2 % O_2 are generally greater than those exposed to 100 % O_2. This effect of decreased temperature dependence with oxygen content is consistent with other *p*-type perovskite materials including $SrFeO_x$ (25,31) and $(Ba,Sr)Fe_{1-x}Ta_xO_3$ (18-21).

A significant dependence on the temperature dependence of film thickness is also evident upon examination of Table 1. In the non-stoichiometric region, $350 \leq T \leq 500$ °C, reduced temperature dependence for the thinner films is indicated by smaller E_A values. Some of these values are even negative, indicating that a decreased temperature actually results in an increased conductance. This phenomenum has previously been reported for other mixed oxide perovskites, albeit at higher temperatures (18-21). Figure 3 illustrates how the film thickness can influence the temperature dependent conduction response. In this case, the thinner 30 nm film has a smaller temperature dependence over a larger temperature range. This may be the result of a higher surface area to volume ratio for the

thinner film resulting in faster bulk oxygen equilibration, or to an effect related to the degree of interfacial stress between the substrate and the film.

All of the E_A values were extracted from isobaric temperature ramps for which the cooling rate was 10 °C/min. At some point during cooling, chemical equilibrium between the film and the surrounding gas mixture cannot be maintained and quenching occurred. The temperature at which quenching begins to occur is dependent on both film composition and thickness, and cooling rate. Figure 4 shows what happens to the resistance response when a $SrFe_{0.25}Co_{0.75}O_x$ film is first equilibrated in air at three different temperatures between 200 - 350 °C in air, cooled by 25 °C at 10°C/min, followed by re-equilibration at the new temperature. At higher temperatures (Figure 4a) the system maintains equilibrium throughout the 10 °C /min cooling rate. Cooling results in an immediate decrease in film resistance resulting from the dominant role of the non-stoichiometric effect (Equation 2). When the temperature is at an intermediate range (Figure 4b), the resistance of the film initially increases with decreasing temperature as would be expected on the basis of thermally activated charge carriers. Once the final temperature is reached, the resistance no longer continues to increase, but instead decreases. This is due to the non-stoichiometric effect, where the film continues to react

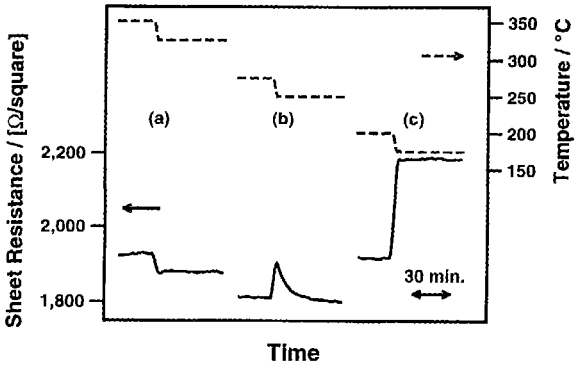

Figure 4: Dynamic temperature response of resistance for 30 nm films of $SrFe_{0.25}Co_{0.75}O_x$ in 20% O_2 for: a) 350-325 °C; b) 275-250 °C; c) 200-175 °C; cooling ramps were conducted at 10 °C/min.

with the oxygen from the surrounding gas mixture, resulting in an increased number of hole charge carriers. At this intermediate temperature range, bulk equilibration still occurs, although too slow for equilibrium to be maintained during the cooling step. At lower temperatures (Figure 4c), quenching occurs and the oxygen stoichiometry of the film does not change. As a result, the balancing of thermal effects can not occur, and the material behaves as a normal semiconductor, where decreasing temperature results in increased resistance.

Oxygen Sensing Properties of $SrFe_yCo_zO_x$ Thin Films

The effects on conductivity of isothermally varying the O_2/N_2 composition at 500 °C was examined for all of the $SrFe_yCo_zO_x$ films. Figure 5 shows a typical example where the O_2/N_2 gas mixture was changed stepwise from 0.2 % O_2 to 100% O_2 and back to 0.2 % O_2. At 500 °C, the resistance response to variations in oxygen composition is rapid and reversible. The response is faster when the O_2 concentration is increasing

uilibration, or to an effect related to the
and the film.
sobaric temperature ramps for which the
ıg cooling, chemical equilibrium between
ıt be maintained and quenching occurred.
to occur is dependent on both film
Figure 4 shows what happens to the
ilm is first equilibrated in air at three
in air, cooled by 25 °C at 10°C/min,
ature. At higher temperatures (Figure 4a)
10 °C /min cooling rate. Cooling results
ılting from the dominant role of the non-
temperature is at an intermediate range
increases with decreasing temperature as
ctivated charge carriers. Once the final
ıger continues to increase, but instead
effect, where the film continues to react

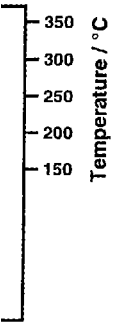

Figure 4: Dynamic temperature response of resistance for 30 nm films of $SrFe_{0.25}Co_{0.75}O_x$ in 20% O_2 for: a) 350-325 °C; b) 275-250 °C; c) 200-175 °C; cooling ramps were conducted at 10 °C/min.

ure, resulting in an increased number of
perature range, bulk equilibration still
maintained during the cooling step. At
rs and the oxygen stoichiometry of the
of thermal effects can not occur, and the
vhere decreasing temperature results in

ilms

y varying the O_2/N_2 composition at 500
ms. Figure 5 shows a typical example
ise from 0.2 % O_2 to 100% O_2 and back
to variations in oxygen composition is
hen the O_2 concentration is increasing

compared to when the O_2 concentration is decreasing. The response time is determined in part by the relatively slow mixing time for the gas mixtures in the chamber. The results of the isothermal variation of O_2/N_2 gas mixtures for the $SrFe_yCo_{1-y}O_x$ set of films are summarized in Figures 6-7. For the $SrFe_{1.0}Co_{0.5}O_x$ and $SrFe_{1.3}Co_{0.2}O_x$ set of films the results are summarized in Figure 8.

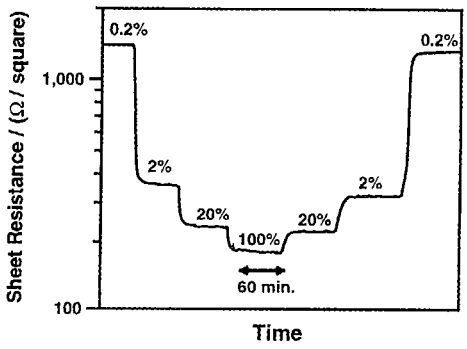

Figure 5: Resistance response to variations in O_2/N_2 gas composition (% O_2) for a 300 nm $SrFe_{0.5}Co_{0.5}O_x$ film at 500 °C .

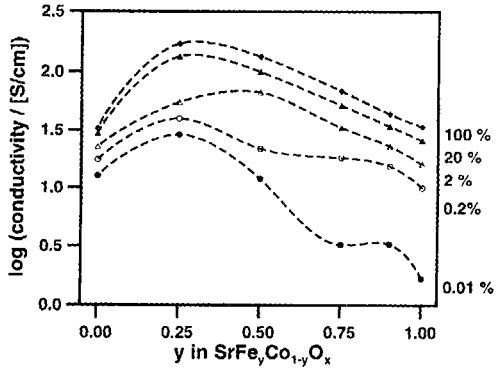

Figure 6: The effects of cobalt substitution and O_2/N_2 gas composition (% O_2) on conductivity for a series of 30 nm $SrFe_yCo_{1-y}O_x$ films at 500 °C.

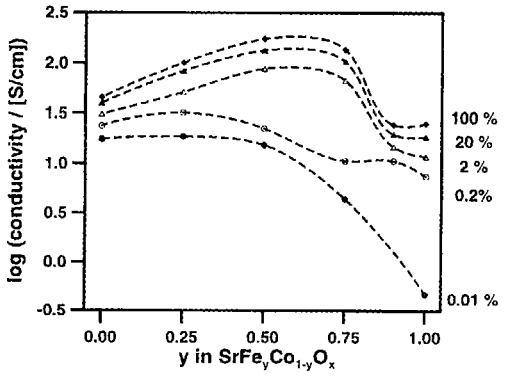

Figure 7: The effects of cobalt substitution and O_2/N_2 gas composition (% O_2) on conductivity for a series of 300 nm thick $SrFe_yCo_{1-y}O_x$ films at 500 °C.

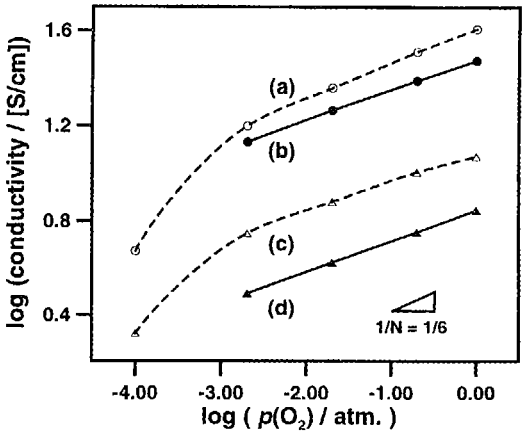

Figure 8: The effects of O_2/N_2 gas composition, $p(O_2)$, on conductivity for the following $SrFe_{1.5-z}Co_zO_x$ films at 500 °C: $SrFe_{1.0}Co_{0.5}O_x$ 30 nm (a), and 300 nm (b); $SrFe_{1.3}Co_{0.2}O_x$ 30 nm (c), and 300 nm (d).

In all cases, exposure to increasing oxygen concentration levels resulted in increased film conductivity as would be expected for *p*-type semiconducting oxides. Film conductivities at 500 °C ranged between 20 - 200 S/cm for films exposed to 100% O_2 atmosphere and 0.4 - 25 S/cm for films exposed to 0.01% O_2. The conductivity of the films increased with increasing cobalt substitution of the $SrFeO_x$ parent material, up to a maximum value. This maximum occurred within the range of composition $SrFe_yCo_{1-y}O_x$ ($0.25 \leq y \leq 0.75$), and was dependent on film thickness and the composition of the gas mixture. $SrCoO_x$ had an unusually low conductivity, possibly as a consequence of its hexagonal crystal structure, which was not observed for the other members of the $SrFe_yCo_{1-y}O_x$ series. The $SrFe_{1.0}Co_{0.5}O_x$ and $SrFe_{1.3}Co_{0.2}O_x$ set of films also showed that

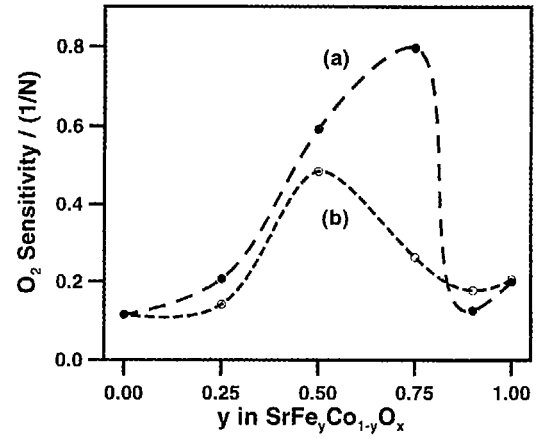

Figure 9: Effects of cobalt substitution on oxygen sensitivity at 500 °C for the $SrFe_yCo_{1-y}O_x$ series of films at two thicknesses: (a) 30 nm (b) 300 nm. Sensitivities were calculated between 0.2 % and 2 % O_2.

cobalt substitution resulted in increased conductivity. There were some subtle differences between the 30 nm series (Figure 6) and the 300 nm (Figure 7) series of films, including differences in the composition for where maximum conductivities were observed. This is

Figure 8: The effects of O_2/N_2 gas composition, $p(O_2)$, on conductivity for the following $SrFe_{1.5-z}Co_zO_x$ films at 500 °C: $SrFe_{1.0}Co_{0.5}O_x$ 30 nm (a), and 300 nm (b); $SrFe_{1.3}Co_{0.2}O_x$ 30 nm (c), and 300 nm (d).

concentration levels resulted in increased or *p*-type semiconducting oxides. Film 200 S/cm for films exposed to 100% O_2 sed to 0.01% O_2. The conductivity of the ion of the $SrFeO_x$ parent material, up to a in the range of composition $SrFe_yCo_{1-y}O_x$ thickness and the composition of the gas ctivity, possibly as a consequence of its observed for the other members of the $Fe_{1.3}Co_{0.2}O_x$ set of films also showed that

Figure 9: Effects of cobalt substitution on oxygen sensitivity at 500 °C for the $SrFe_yCo_{1-y}O_x$ series of films at two thicknesses: (a) 30 nm (b) 300 nm. Sensitivities were calculated between 0.2 % and 2 % O_2.

tivity. There were some subtle differences 0 nm (Figure 7) series of films, including ium conductivities were observed. This is

possibly an effect of the increased role of interfacial stress between the film and the substrate for the thinner films.

The sensitivity of the film to oxygen, 1/N as measured by $\Delta\log\{\text{conductivity}\}/\Delta\log\{p(O_2)\}$ (18), ranged from $0.05 \leq 1/N \leq 0.9$. For some films, including $SrFe_{0.5}Co_{0.5}O_x$ and $SrFe_{0.75}Co_{0.25}O_x$, enhanced oxygen sensitivity was observed over narrow $p(O_2)$ regions. This was evident from anomalous large spacings between consecutive isobar lines in Figures 6-7, and from an increased slope between two consecutive points in the $\log\{\sigma\}$ vs $\log\{p(O_2)\}$ plots shown in Figure 8.

Enhanced oxygen sensitivity of $SrFeO_{2.5+x}$ has been previously attributed to phase transitions between the brownmillerite and cubic perovskite phases (25). At 500 °C this phase transition is expected to occur at $0.005 \leq p(O_2) \leq 0.05$ atmosphere (25-27). Liu *et al.* (32) have also identified a similar phase transition for $SrFe_{0.2}Co_{0.8}O_x$ below 750 °C for $0.05 \leq p(O_2) \leq 0.20$ atmosphere. The sensitivity of the films to oxygen between $0.002 \leq p(O_2) \leq 0.02$ atmosphere for the series of $SrFe_yCo_{1-y}O_x$ films is shown in Figure 9. For the 300 nm films, high oxygen sensitivity is observed for the both $SrFe_{0.5}Co_{0.5}O_x$ and $SrFe_{0.75}Co_{0.25}O_x$, whereas it is only observed for $SrFe_{0.5}Co_{0.5}O_x$ for the 30 nm films. This demonstrates that thickness may also play a role in determining the sensitivity of the film to oxygen.

CONCLUSIONS

It has been demonstrated that thin films of $SrFe_yCo_zO_x$ grown by PLD exhibit novel conductivity responses with respect to variation in both temperature and gas composition. Due to the balancing of thermal effects, it is possible to obtain a conduction response which has a negligible temperature dependence between $200 \leq T \leq 500$ °C. This effect was most pronounced for the perovskites with compositions $SrFe_{0.25}Co_{0.75}O_x$ and $SrFe_{0.5}Co_{0.5}O_x$. Thinner films (30 nm) show a greater temperature independence than the thicker (300 nm) films at temperature between $350 \leq T \leq 500$ °C . All of the $SrFe_yCo_zO_x$ films showed reversible *p*-type gas sensor responses at 500 °C to variations in O_2/N_2 gas mixtures. Regions of enhanced oxygen sensitivity over narrow $p(O_2)$ ranges were attributed to phase transitions between the cubic perovskite and brownmillerite phases.

ACKNOWLEDGEMENTS

The authors are grateful to G. Pleizier for the SEM analysis of the thin films, and V. Boyko for the elemental analysis measurements by ICP-AES.

REFERENCES

1. Y. Teraoka, H.-M. Zhang, S. Furukawa and N. Yamazoe, *Chem. Letters* **1985**, 1743 (1985).
2. Y. Teraoka, T. Nobunaga and N. Yamazoe, *Chem. Letters* **1988**, 503 (1988).
3. Y. Teraoka, H.M. Zhang, K. Okamoto and N. Yamazoe, *Mat. Res. Bull.* **23**, 51 (1988).
4. V.V. Kharton, E.N Naumovitch and A.V. Nikolaev, *J. Membrane Science* **111**, 149 (1996).
5. V.V. Kharton, V.N. Tikhonovitch, L. Shuangbao, E.N. Naumovitch, A.V. Kovalevsky, A.P. Viskup, I.A. Bashmakov and A.A. Yaremchenko, *J. Electrochem. Soc.*, **145**, 1363 (1998).
6. L.V. Kokhanovskii, V.V. Vashuk, E.F. Vil'kotshaya, S.I. Vitushko and M.V. Zinkevich, *Inorganic Materials*, **35**, 282 (1999).
7. L. Qiu, T.H. Lee, L.M. Jiu, Y.L. Yang and A.J. Jacobson, *Solid State Ionics* **76**, 321 (1995).
8. T. Armstrong , F. Prado, Y. Xia and A. Manthiram, *J. Electrochem. Soc.* **147**, 435 (2000).
9. S. Guggilla and A. Manthiram, *J. Electrochem. Soc.* **144**, L120 (1997).
10. J.W. Stephenson, T.R. Armstrong, R.D. Carneim, L.R. Pederson and W.J Weber, *J. Electrochem. Soc.* **143**, 2722 (1996).
11. U. Balachandran, B. Ma, P.S Maiya, R.L. Mieville, J.T. Dusek, J.J. Picciolo, J. Guan, S.E. Dorris and M. Liu, *Solid State Ionics* **108**, 363 (1998).
12. B. Ma, U. Balachandran, J.H. Park and C.U. Segre, *Solid State Ionics* **83**, 65 (1996).
13. B. Ma, U. Balachandran, J.H. Park and C.U. Segre, *J. Electrochem. Soc* .**143**, 1736 (1996).
14. B. Ma and U. Balachandran, *Solid State Ionics* **100**, 53 (1997).
15. B. Ma and U. Balachandran, *J. Electroceramics* **2**, 135 (1998).
16. B.J. Mitchell, J.W. Richardson, C.D. Murphy, B. Ma, U. Balachandran, J.P. Hodges and J.D. Jorgensen, *Mater. Res. Bull.* **35**, 491 (2000).
17. B. Ma and U. Balachandran, *Mater. Res. Bull.* **33**, 223 (1998).
18. P.T. Moseley and A.J. Crocker, Chapt. 4 in *Sensor Materials*, Institute of Physics Publishing Ltd, London (1996).
19. P.T. Moseley and D.E. Williams, *Polyhedron* **8**, 1615 (1989).
20. D.E. Williams, B.C. Tofield and P. McGeehin, *European Patent* EP62-994 and *US Patent* 4,454,494 (1982).
21. R. Moos, W. Menesklou, H.-J. Schreiner and K.H. Härdtl, *Sensors and Actuators B* **67**, 178 (2000).
22. M.L. Post, B.W. Sanders and P. Kennepohl, *Sensors and Actuators B*, **13-14**, 272 (1993).
23. M.L. Post, J.J. Tunney and J. Yao, in *Chemical and Biological Sensors and Analytical Electrochemical Methods*, A.J. Ricco, M.A. Butler, P. Vanysek, G. Horvai and A.F. Silva, Editors, PV 97-19, p. 889, The Electrochemical Society Proceedings Series, Pennington, NJ (1997).
24. M.L. Post, J.J. Tunney, D. Yang, X. Du and D.L. Singleton, *Sensors and Actuators B*, **59**, 190 (1999).
25. J.J. Tunney and M.L. Post, *J. Electroceramics* **5**, 63 (2000).

26. Y. Takeda, K. Kanno
Bando, *J. Solid State*
27. J. Mizusaki, M. Okay
(1992).
28. J.P. Hodges, S. Short
Kimball, *J. Solid Sta*
29. Y. Takeda, R. Kanno
Allg. Chem. **540/541**
30. H. Fjellvag, B.C. Hau
31. J. Hombo, Y. Matsum
32. L.M. Liu, T.H. Lee, L
(1996).

nd N. Yamazoe, *Chem. Letters* **1985**, 1743

e, *Chem. Letters* **1988**, 503 (1988).
d N. Yamazoe, *Mat. Res. Bull.* **23**, 51

Nikolaev, *J. Membrane Science* **111**, 149

angbao, E.N. Naumovitch, A.V.
ov and A.A. Yaremchenko, *J. Electrochem.*

il'kotshaya, S.I. Vitushko and M.V.
(1999).
d A.J. Jacobson, *Solid State Ionics* **76**, 321

anthiram, *J. Electrochem. Soc.* **147**, 435

hem. Soc. **144**, L120 (1997).
arneim, L.R. Pederson and W.J Weber, *J.*

Mieville, J.T. Dusek, J.J. Picciolo, J. Guan,
108, 363 (1998).
U. Segre, *Solid State Ionics* **83**, 65 (1996).
U. Segre, *J. Electrochem. Soc* .**143**, 1736

nics **100**, 53 (1997).
amics **2**, 135 (1998).
phy, B. Ma, U. Balachandran, J.P. Hodges
491 (2000).
Bull. **33**, 223 (1998).
n *Sensor Materials*, Institute of Physics

ron **8**, 1615 (1989).
ehin, *European Patent* EP62-994 and *US*

nd K.H. Härdtl, *Sensors and Actuators B*

l, *Sensors and Actuators B*, **13-14**, 272

nical and Biological Sensors and
Ricco, M.A. Butler, P. Vanysek, G.
p. 889, The Electrochemical Society
).
d D.L. Singleton, *Sensors and Actuators B*,

nics **5**, 63 (2000).

26. Y. Takeda, K. Kanno, T. Takada, O. Yamamoto, M. Takano, N. Nakayama and Y. Bando, *J. Solid State Chem.* **63**, 237 (1986).
27. J. Mizusaki, M. Okayasu, S. Yamauchi and K. Fueki, *J. Solid State Chem.* **99**, 166 (1992).
28. J.P. Hodges, S. Short, J.D. Jorgensen, X. Xiong, B. Dabrowski, S.M. Mini and C.W. Kimball, *J. Solid State Chem.* **151**, 190 (2000).
29. Y. Takeda, R. Kanno, T. Takada, O. Yamamoto, M. Takano and Y. Bando, *Z. Anorg. Allg. Chem.* **540/541**, 259 (1986).
30. H. Fjellvag, B.C. Hauback and R. Bredesen, *J. Mater. Chem.* **1997**, 2415 (1997).
31. J. Hombo, Y. Matsumoto and T. Kawano, *J. Solid State Chem.* **84**, 138 (1990).
32. L.M. Liu, T.H. Lee, L. Qiu, Y.L. Yang and A.J. Jacobson, *Mater. Res. Bull.* **31**, 29 (1996).